J Mol Model (2012) 18:2599–2611
DOI 10.1007/s00894-011-1275-1

ORIGINAL PAPER

Exploration of the binding of curcumin analogues to human P450 2C9 based on docking and molecular dynamics simulation

Rongwei Shi · Yin Wang · Xiaolei Zhu · Xiaohua Lu

Received: 28 April 2011 / Accepted: 9 October 2011 / Published online: 12 November 2011

Abstract Molecular docking and molecular dynamics (MD) simulations are used to investigate the interactions of curcumin analogues (CAs) with human cytochrome P450 2 C9 (CYP2C9 or 2 C9) and the conformations of their binding sites. In order to examine conformations of CAs/2 C9 and interaction characteristics of their binding sites, RMSDs, RMSFs, and B-factors are computed, and electrostatic and hydrophobic interactions between CAs and 2 C9 are analyzed and discussed. Results demonstrate that the most CAs studied lie 4∼15 Å above the heme of CYP2C9. The presence of CAs makes some residues in bound CYP2C9s become more flexible. In the binding sites of A0/2 C9 and C0/2 C9, the formation of H-bond networks (or CA-water-residue bridges) enhances the interactions between CAs and 2 C9. The stronger inhibitory effects of A0, B0, and C0 on 2 C9 can be ascribed to stronger electrostatic and hydrophobic interactions in the binding sites of CAs/2 C9.

Keywords Binding site · Curcumin analogues · CYP2C9 · Docking · Molecular dynamics simulation

Electronic supplementary material The online version of this article (doi:10.1007/s00894-011-1275-1) contains supplementary material, which is available to authorized users.

R. Shi · Y. Wang · X. Zhu (✉) · X. Lu (✉)
State Key Laboratory of Materials-Oriented Chemical Engineering, College of Chemistry and Chemical Engineering, Nanjing University of Technology, Nanjing 210009, China
e-mail: xlzhu@njut.edu.cn
e-mail: xhlu@njut.edu.cn

Introduction

Cytochrome P450 (CYP or P450) enzymes are heme-containing monooxygenases. They can participate in many reactions [1–4] contribute extensively to the metabolism of xenobiotics and endogenous compounds, such as drugs, environmental pollutants, and carcinogens [5]. Especially, 1A2, 2 C19, 2 C9, 2D6, 2E1, and 3A4/5 contribute to the metabolism of about 90% drugs in current clinical use [6–8]. Extensive research on understanding the mechanism of P450-catalyzed reactions have been performed [9].

CYP2C9(or 2 C9), one of the major enzymes of CYPs, contributes to the metabolism of about 16% of all drugs and is responsible for phase I metabolism of these drugs [6]. Human cytochrome P450 2 C9 (CYP2C9) is embedded mainly in hepatocytes of liver. This enzyme may be involved in potentially unfavorable drug-drug interactions or drug toxicity. Furthermore, CYP2C9 displays atypical kinetics with several substrates such as flurbiprofen, dapsone, naproxen [10–12]. Thus, it is necessary to explore how these drugs or substrates interact with 2 C9 so as to obtain some useful information for the drug's therapeutic efficacy or toxicity in clinical application.

In recent years, several structures of mammalian CYP enzymes such as CYP3A4 [13, 14], CYP2C9 [15, 16], CYP2B4 [17], CYP2A6 [18], CYP2C8 [19], and CYP2C5 [20] have been solved. Moreover, there are many reports about the structure/metabolism relationship, binding model, and interaction prediction for 2 C9 with drug molecules [6, 21–28]. Molecular docking study on the affinity of 2 C9 for imrecoxib has been performed using InsightII/Affnity program by Li et al. [29]. Experimentally, the inhibition capacity of five hydroxywarfarin metabolites on S-warfarin

metabolized by CYP2C9 has been investigated by Jones et al. [30]. Their results indicated that hydroxywarfarin does limit the metabolic capacity toward S-warfarin and this limitation process is produced by competitive inhibition.

Curcumin, a natural polyphenol derived from turmeric (*Curcuma longa*), is a yellow pigment generally used as spice, flavoring agent, food preservation, coloring agent [31, 32]. Curcumin is a component of many drug agents, which exhibit antifungal, anti-inflammatory, antiviral, antibacterial, anticancer, and antioxidant and has been potentially applied to medical treatment for diabetes, malignant diseases, allergies, arthritis, Alzheimer's disease, and other chronic illnesses [33]. Moreover, a number of research works have shown that curcumin reduces blood cholesterol [34–40], inhibits platelet aggregation [41, 42], rheumatoid arthritis [43], and HIV replication [44–48], protects from liver injury [49]. Some experiments in vivo or in vitro animal studies have argued that curcumin can regulate activity of several drug-metabolism enzymes such as CYP1A1[50, 51], CYP2B1[50, 51], CYP3A [52]. There are also some reports about curcumin or curcumin analogues (CAs) interacting with P450 isozymes and other enzyme [53–57].

Curcumin has two invertible enol and keto structures as shown in Fig. SI-1. Curcumin has been proved to have strong inhibition to 2 C9 and CYP3A4. Due to the active methylene group, curcumin is not stable above pH of 6.5 [58]. So Vermeulen's group [55] designed some CAs. Their results demonstrated that some of them have stronger inhibition to five major recombinant human drug-metabolizing CYPs (CYP3A4, CYP2C9, CYP2D6, CYP2B6, CYP1A2). However, interaction mechanisms of these CAs with 2 C9 at atomic level are not clear.

Herein, the interactions of CAs with CYP2C9 [15] in binding sites are explored by molecular docking and MD simulation techniques. Results demonstrate that the presence of CAs changes the flexibility of some residues in bound CYP2C9s. In binding sites of CAs/2 C9, some CAs undergo interesting conformational changes. The stronger electrostatic and hydrophobic interactions of A0/2 C9, B0/2 C9, and C0/2 C9 are supported by the stronger inhibitory activities of CAs to 2 C9. These studies will be valuable for the design of new CAs.

Computational methods

Molecule models of CYP2C9 and its ligands

The model of CYP2C9 was established based on the C terminal truncated X-ray crystal diffraction structure of warfarin-bounded CYP2C9 complex (1OG2, resolution 2.6 Å). [15] The crystal structure of CYP2C9 is comprised of two similar subchains. One subchain was chosen to apply to the following docking and MD simulations. In this work, we selected five CAs, that is, A0, B0, B12, C0, C2. These CAs were built up using 3D graphical software, and then were optimized at the B3LYP/6-31 G(d) level using Gaussian 09 program package [59].

Docking

The molecular docking of CAs to 2 C9 was carried out using Autodock 4.0 program [60]. Before docking, polar hydrogen atoms were added to CYP2C9 and Kollman all-atom charges were also assigned to this enzyme. During docking process, CYP2C9 was kept rigid, but all torsional angles of CAs were free in order to execute flexible docking.

The grid maps were calculated using Autogrid and chosen to be sufficiently large to accommodate the active sites and the key parts of CYP2C9. Then, the three dimensions of the grid were set to 100 Å×98 Å×98 Å with 0.375 Å spacing value. During the docking process of CAs to CYP2C9, the empirical free energy function and the Lamarckian genetic algorithm were employed. The genetic algorithm runs of 200 were performed with maximum of energy evaluations to 25,000,000 for each ligand. The internal electrostatic energy was also calculated and the docking results were clustered based on the root-mean-square deviation (RMSD) criterion of 2.0 Å.

MD simulations

According to the docking results, MD simulations on CAs/2 C9 were performed with the GROMOS96 force field [61, 62] using GROMACS 3.3.3 package [63, 64]. The CAs topology files were created by the program PRODRG [65]. During MD simulations, each of the complexes in an octahedron box was solvated with the simple point charge (SPC) water model [66, 67]. To neutralize each system, three Na^+ ions were added in each 2 C9/CA complex. In order to keep the simulation system in a stable environment, the Berendsen temperature was kept at 300 K and the pressure coupling was maintained to 1 bar (the Berendsen coupling constants [68] were set to 0.1 ps). The isothermal compressibility was chosen as 4.5×10^{-5} bar^{-1} for water simulations. The bond length was constrained by the LINCS algorithm [69]. Electrostatic interactions were calculated employing the particle mesh Ewald (PME) method [70]. The Lennard-Jones interactions were also computed with a cutoff distance of 14 Å. For each system, the minimum distance between the complex and the box walls was taken as 10 Å. The leap-frog algorithm with a time step of 2 fs was applied and the periodic boundary condition was employed. Furthermore, each simulation

system contains 4752 protein atoms and 16,670 solvent molecules included in a $13\times13\times9$ nm^3 box.

For energy minimization of each system, the structure of complex was fixed, all ions and water molecules were minimized by using the steepest descent method to reach the convergence criterion of 1000 kJ/(mol,nm). After that, position restrained dynamics simulation was carried out on each system. Proteins, ligands, and water molecules were coupled separately to a temperature bath of 300 K using a coupling time of 0.1 ps. Finally, 10 ns MD simulation was carried out for each of CAs/2 C9.

Results and discussion

Docking

The structures of five CAs, which are derived from benzylidine, are displayed in Fig. 1. In CAs, the ketone group is an electron-donating group and the aromatic ring can be considered as a hydrophobic group. The docking energies and binding energies of favorable docking conformations are displayed in Table 1. The superimposed docking conformations of CAs in CYP2C9 are shown in Fig. SI-2. As shown in Fig SI-2, most CAs studied lie 4~15 Å above the heme of CYP2C9, which is similar to the results from previous investigations [15, 16, 28, 71, 72]. And the binding cavity for these CAs is composed of the helix A, F-G loop, helix I and heme group. The detailed docking and binding information are shown in Fig. 2, where the hydrophobic residues located within the range of ~4 Å around CAs are shown in lines. As shown in Fig. 2, hydroxyl oxygen or ketonic oxygen in each CA forms hydrogen bonds with surrounding residues. In addition, there exist hydrophobic interactions in the docking conformations. The hydrophobic pocket of B0-2 C9 consists of ten residues of Phe100, Leu102, Ala103, Ala106, Phe114, Leu208, Ile213, Val237, Val292 and Phe476 while the hydrophobic pockets of A0, B12, C0, and C2 have five same residues (Phe100, Ala103, Leu208, Ile213, Phe476).

MD simulations

Stability of CAs/2 C9 and residue flexibility of the bound CYP2C9s

The favorable docking structures of CAs/CYP2C9 are taken as the initial conformations in MD simulations. MD simulations have been performed on these complexes to explore the binding interactions between CAs and 2 C9, and the conformational changes of bound 2 C9 and CAs. Figure 3 displays the RMSD from the initial structures of total Cα atom with time evolution. For comparison, the total Cα RMSDs of the free CYP2C9 (PDB code: 1OG2 [15]) are also shown in Fig. 3. As shown in Fig. 3, the stable RMSDs for all systems illustrate that these systems reach equilibrate after ~7 ns.

The root-mean-square fluctuation (RMSF) from the averaged structure is usually as a reference to evaluate the convergence of MD simulation. Figure SI-3 displays the averaged atomic fluctuations of residues for bound- and unbound-2 C9 with time evolution. As shown in Fig. SI-3, for CYP2C9s of most complexes, their RMSFs reveal that

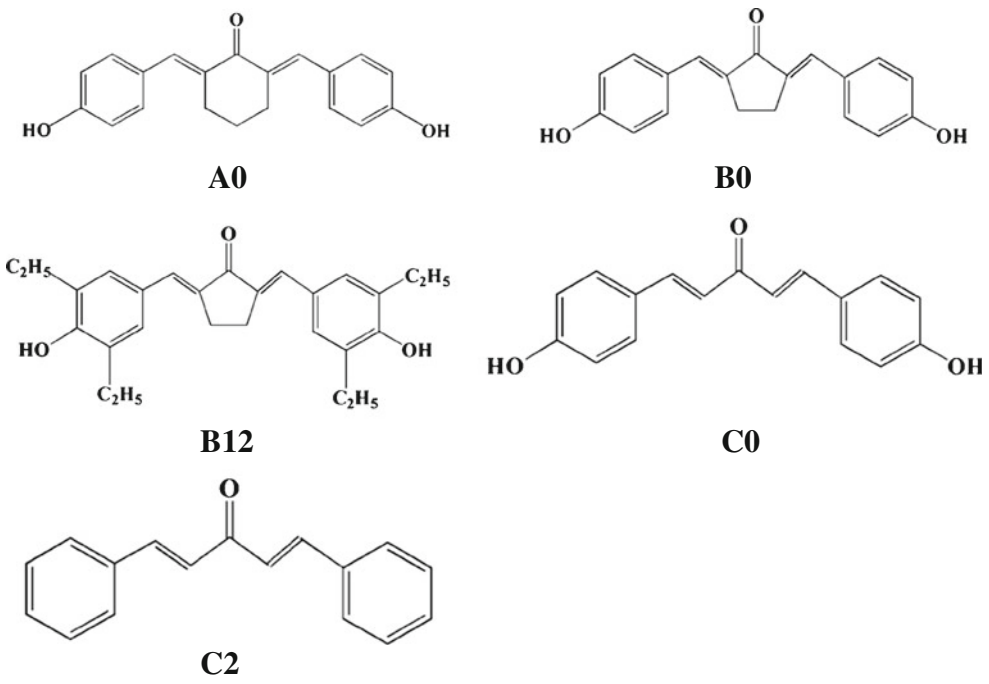

Fig. 1 Chemical structures of curcumin analogues

Table 1 Binding and docking energies of CAs and2C9 calculated by AutoDock

Curcumin analogues	Bingding energy (kcal/mol)	Docking energy (kcal/mol)	Inhibition constant (μM,298.15 K)
A0	−7.70	−8.65	2.28
B0	−7.18	−8.25	5.41
B12	−7.47	−9.73	3.36
C0	−7.36	−8.93	4.01
C2	−6.82	−7.82	9.95

the residues with higher flexibilities distribute in B-C loop (~Arg108 and Arg132), F-G loop (~Trp212 and Tyr225), H-I loop (~Lys275), long loop Lys399-Lys423 and C terminal loop (~Lys465), which are consistent with the results obtained from Afzelius et al. [9].

B-factors reflect [73] the thermal mobility or the fluctuation of the individual residues or atoms of the protein. In order to further examine the movement of residues in 2 C9/CAs after MD simulations, the B-factors for each system are computed and compared with experi-

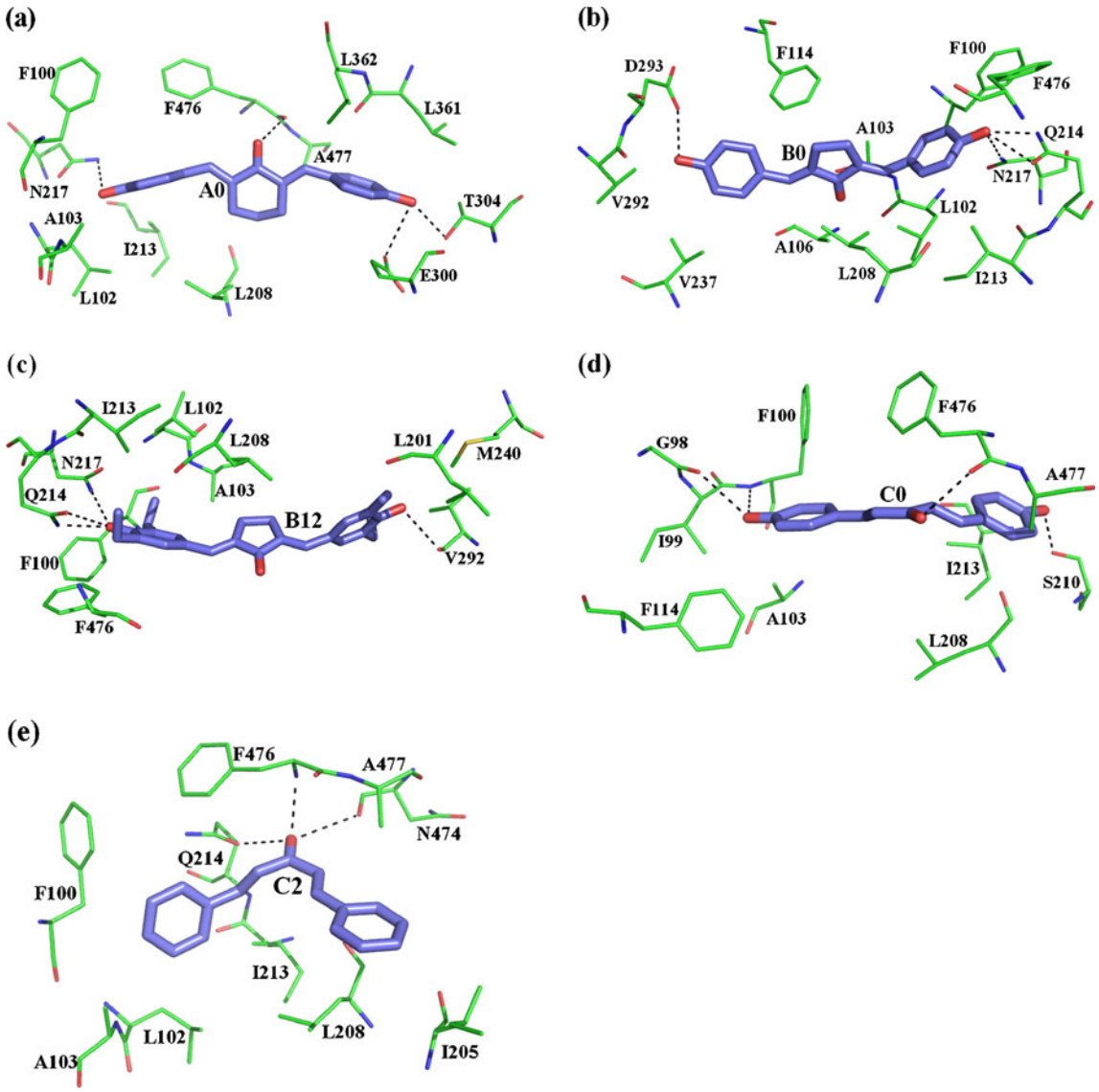

Fig. 2 The binding modes of CYP2C9 docking with curcumin analogues of A0 (**a**), B0 (**b**), B12 (**c**), C0 (**d**), and C2 (**e**). Carbon atoms of curcumin analogues and the surrounding hydrophobic residues within the range of 4 Å are colored in purple and green, respectively. Dotted black lines represent polar interactions or hydrogen bonds

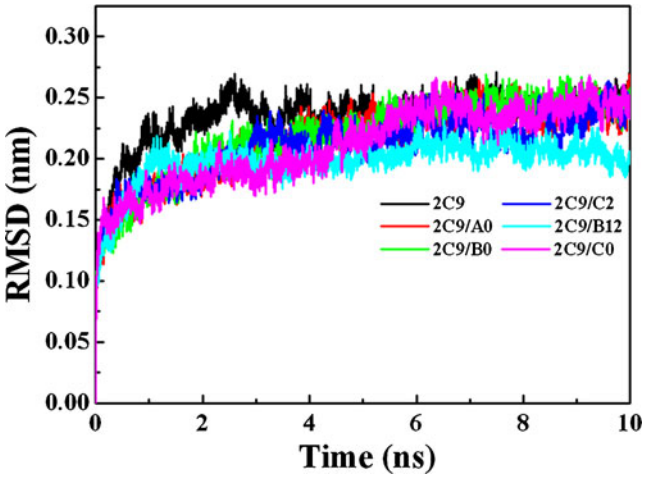

Fig. 3 Time dependence of the Cα RMSDs from the crystal structure of 2 C9 and complexes (2 C9/A0, 2 C9/B0, 2 C9/C2, 2 C9/B12, 2 C9/C0) during MD simulations

mental values. Figure 4 shows the calculated B-factors of B0-bound 2 C9 and experimental values of 2 C9 obtained from X-ray crystal structure [15]. The B-factors of other CAs/2 C9 are displayed in Fig. SI-4. It is observed from Fig. 4 and Fig. SI-4 that for most residues, the experimental B-factors are larger than those obtained from MD simulations. In the case of B0/2 C9, the B-factors from MD simulations are in qualitatively agreement with experimental values. However, B-factors for residues around Lys275 and Lys423 are significant larger than corresponding experimental values, suggesting these residues have high flexibility, which is in accordance with the results from RMSF.

Conformations of CAs in the binding sites

Figure 5a displays the total atom RMSDs of some CAs inside the binding pocket as a function of time, while Fig. 5b represents structural superposition for the snapshots

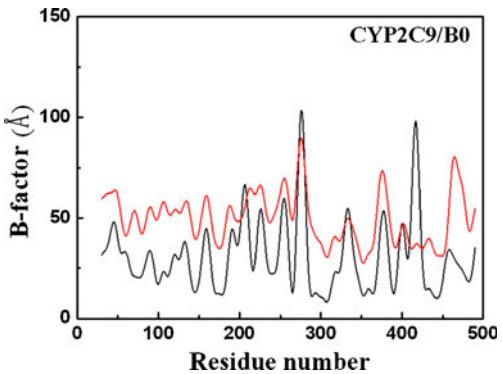

Fig. 4 The experimental residue B-factors (red curve) of 2 C9 obtained from X-ray crystal structure and calculated values of bound 2 C9 in 2 C9/B0 (black curve) from the last 3 ns of MD simulations

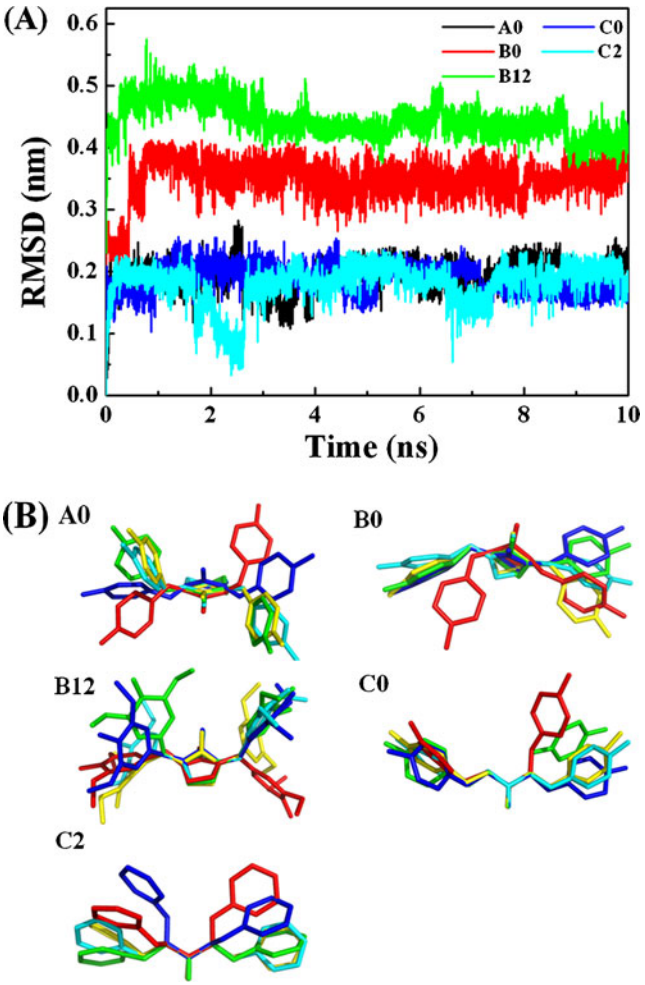

Fig. 5 (**a**) Total atom RMSDs for A0 (black), B0 (red), B12 (green), C0 (blue), and C2 (cyan). To enhance the visual clarify, the curves of B0, B12 and C0 are shifted upward 0.15, 0.23, and 0.02 nm respectively. (**b**) Structural superpositions for the snapshots of some typical CAs isolated from the MD trajectories. The snapshots of A0 are obtained at 0 ns (red), 2 ns (green), 3.5 ns (blue), 8 ns (yellow), 10 ns (cyan), respectively. The snapshots of B0 are calculated at 0 ns (red), 2 ns (green), 6 ns (blue), 8 ns (yellow), 10 ns (cyan), respectively. The snapshots of B12 are calculated at 0 ns (red), 2 ns (green), 4 ns (blue), 8 ns (yellow), 10 ns (cyan), respectively. The snapshots of C0 are obtained at 0 ns (red), 2.5 ns (green), 5 ns (blue), 6.5 ns (yellow), 10 ns (cyan), respectively. The snapshots of C2 are obtained at 0 ns (red), 1.5 ns (green), 2.5 ns (blue), 7 ns (yellow), 10 ns (cyan), respectively

of corresponding CAs in CAs/2 C9 at different times. Obviously, the RMSDs for some CAs exhibit significant changes, which may imply that CAs undergo conformational changes in the binding sites of CAs/CYP2C9. For example, the RMSD values of B0 sharply increase near 1 ns, and then keep stable after 1 ns. Interestingly, it is noted from Fig. 5b that B0 exhibits conformational change from U-bend to extended structures near 1 ns, which is consistent with the results from Fig. 5a. The significant increase (Fig. 5a) of RMSDs for C2 near 2.8 ns also

corresponds to its conformational transformation from U-bend to extended structures in Fig. 5b. For B12, its conformation appears to be an extended structure at 0 ns, then, it swings between U-bend and extended structures within 2~9 ns, finally, it becomes U-bend structure after 9 ns as shown in Fig. 5.

Interactions in CAs/2C9 binding sites

LIGPLOT, a program automatically generating 2D schemes of protein-drug complexes from MD simulations, is applied to examine the hydrogen bonds and hydrophobic interactions between CAs and CYP2C9 as shown in Fig. 6a. It can be obviously seen from Fig. 6a that there is an H-bond network formed by some water molecules, A0, and residues around the binding site. There exist two hydrogen bonds between A0 and waters after MD simulations. These two hydrogen bonds form between ketone oxygen atom (O21) of A0 and oxygen atoms of waters as shown in Fig. 6a. The radial distribution function (RDF) for the ketone oxygen atom (O21) of A0 and oxygen atoms of waters is displayed in Fig. 6b. The RDF for the O21-OW (Fig. 6b) shows an

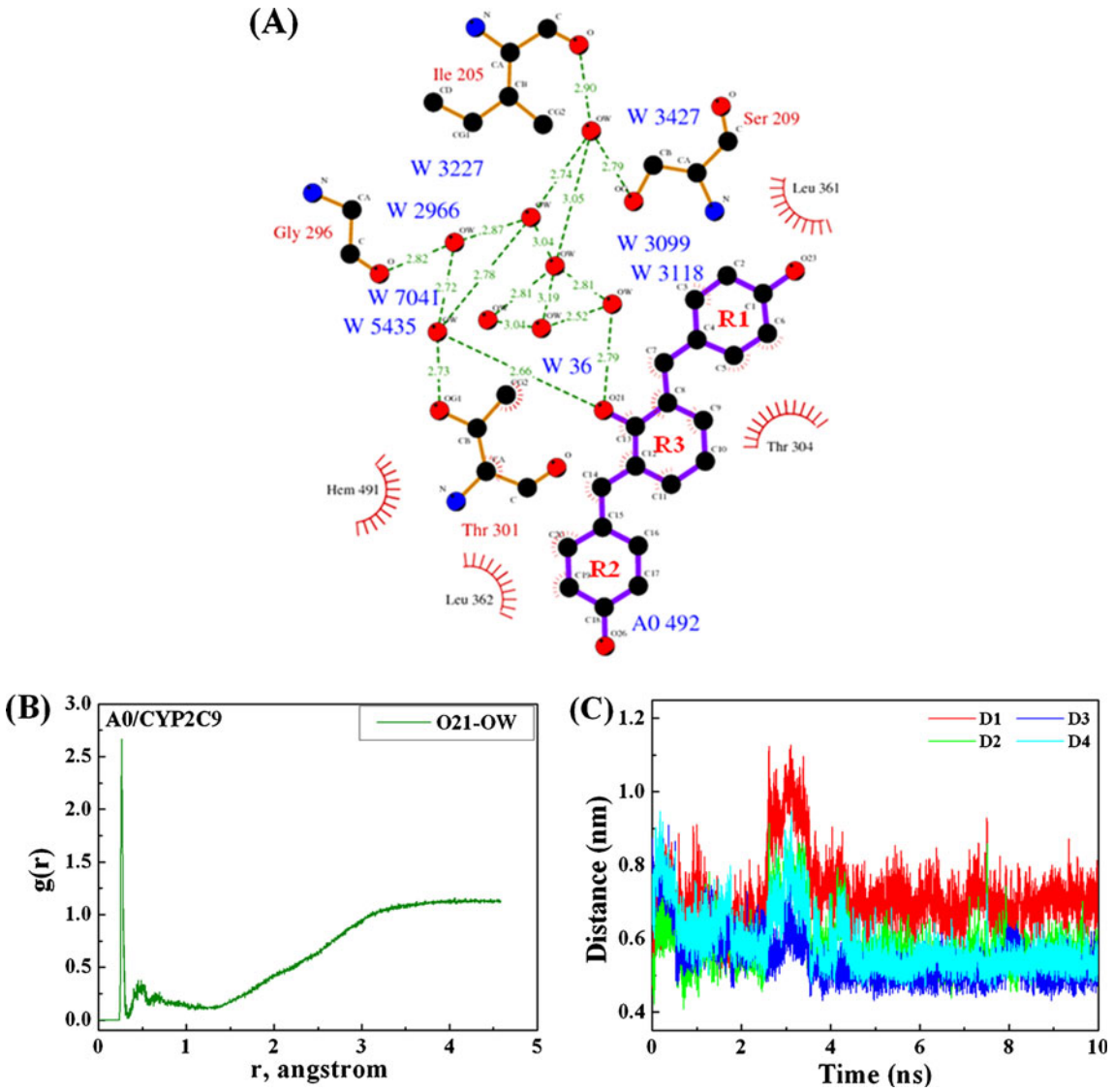

Fig. 6 (**a**) Two-dimensional schematic representations of hydrogen bond and hydrophobic interaction for the binding site of CYP2C9/A0. W36, W2966, W3099, W3118, W3227, W3427, W5435 and W7041 represent the water molecules which hold A0 and residues around binding site together by hydrogen bonds. Dashed lines represent hydrogen bonds and spiked residues form hydrophobic interactions. And the distances of hydrogen bonds are labeled in the middle of the dash lines. (**b**) Radial distribution function for O21-OW (oxygen atoms (OW) of waters and ketone oxygen (O21) of A0). (**c**) The mass-center distances associated with hydrophobic interactions of A0 in the binding site of CYP2C9 versus MD simulation time. D1, D2, and D4 represent the distances between R1 ring of A0 and the main chains of Leu362, Leu361 and Thr304, respectively. D3 displays the distance between main chain of Leu362 and R3 ring of A0

obvious peak at about 0.25 nm, which confirms the formation of hydrogen bond between ketone oxygen atom (O21) of A0 and oxygen atoms of waters. Meanwhile, the hydrophobic interactions between 2 C9 and A0 are estimated based on the time dependences of the related mass-center distances. As shown in Fig. 6c, D1∼D4 keep stable after ~4 ns, which reveal that the hydrophobic interactions are favorable to stabilizing binding sites of A0/2 C9. Figure SI-5 shows the snapshots of the hydrogen bonds network near binding site of A0/CYP2C9 at 2, 2.5, 3.5, 6, 8, 10 ns, respectively. Interestingly, as shown in Fig. SI-6, these water molecules held ketone oxygen atom (O21) of A0 and adjacent residues of 2 C9 together via hydrogen bonds. In addition, several water molecules in the hydrogen-bond network always exchange with other water molecules with time evolution. Clearly, the presence of these water bridges is important for stabilization of 2 C9-A0 binding site.

Although the structure difference between B0 and A0 is small, the binding mode of CYP2C9-B0 (Fig. 7) obtained from MD simulations is different from that of CYP2C9-A0. As shown in Fig. 7a and Fig. SI-6, there exist three hydrogen bonds between B0 and surrounding amino acids (Asn204, Asn217 and Ala103). These hydrogen bonds can be represented by O24(A0)-ND2(Asn204), O15(A0)-ND2 (Asn217), and O15(B0)- N(Ala103), respectively. The distances associated with these hydrogen bonds with time evolution are displayed in Fig. 7b. The two hydrogen bonds are stable after ~2 ns with average lengths of 0.31 and 0.29 nm for O15(A0)-N(Ala103) and O15(A0)-ND2 (Asn217), respectively, which are favorable to stabilizing the B0/CYP2C9 binding site. In addition, hydrophobic contacts have also been analyzed between B0 and the hydrophobic residues (Phe100, Leu102, Ala106 and Pro367) in Fig. 7c. Clearly, the hydrophobic interactions are favorable to stabilization of B0/CYP2C9 binding site. On the other hand, Fig. SI-7 shows snapshots of the CYP2C9-B0 binding site at different times. Obviously, the ketone oxygen and hydroxyl oxygen of B0 form stable hydrogen bonds with amide nitrogens of some residues (Asn217 and Ala103) and oxygens of waters with time evolution. The above analyses reveal that hydrophobic and H-bond interactions result in relatively stable extended conformation of B0 in the B0/2 C9 binding site. On the other hand, the ketone oxygen of B0 forms stable hydrogen bonds with amide nitrogens of some residues (Asn217 and Ala103) during MD simulation, resulting in the smaller flexibilities of residues (Asn217 and Ala103), which is consistent with the results reflected from Fig. SI-4.

Structurally, B0 and B12 are identical except for the presence of C_2H_5 substitutions. In the case of B0 in B0/2 C9, the substituted C_2H_5 groups are adjacent to hydroxyl groups in B12, which may cause steric hindrance and prevent the H-bonds between hydroxyl groups and adjacent residues or water as shown in Fig. SI-7a. However, there are some hydrophobic contacts. Figure SI-7b shows the mass-center distances between the hydrophobic residues (G296, F476, L362, F100, A103) and one side benzene ring (ben), center cyclopentanone group (pent), one substituted methyl group (CH_3) in benzene ring of B12 with time evolution. Clearly, these hydrophobic interactions are relatively weaker.

As shown in Fig. 8, the interactions in C0-2 C9 binding site are similar to those of A0-2 C9. Figure 8a shows that there are two hydrogen bonds between the ketone oxygen of C0 and water/residue of 2 C9. Figure 8b represents the H-bond distance between O13 of C0 and one water (W3466) (or one nitrogen (ND2) of N217) with time evolution, which reveals that these two hydrogen bonds are stable after 5.6 ns and 1 ns, respectively. Figure 8c displays the mass-center distances between the hydrophobic residues (F100, F476, F69, L366, L388, V113) and carbon chains (chain1 and chain2) at both sides of the ketone group, two terminal benzene rings (ben1 and ben2) of C0 with time evolution. Their hydrophobic interactions become stable after 7.7 ns. Obviously, the hydrogen bond and hydrophobic interactions between C0 and 2 C9 are favorable for stabilizing the C0/2 C9 binding site.

In the case of C2/2 C9, as shown in Fig. SI-8a and Fig. SI-8b, there is one stable hydrogen bond between ketone oxygen of C2 and oxygen of water, which held C2, water, and residues (Phe100 and Gly98) of 2 C9 together. There are weak hydrophobic interactions between the two phenyl rings of C2 and some residues of 2 C9 as shown in Fig. SI-8c.

The final structures of binding sites of A0/CYP2C9 and B0/CYP2C9 are shown in Fig. 9. The final conformations for the binding sites of other CAs/CYP2C9 complexes are displayed in Fig. SI-9.

Electrostatic properties caused by polar side chains and charged residues play roles in the stability of protein and protein-ligand [74, 75]. Therefore, the electrostatic potential of the binding sites as shown in Fig. 10 and Fig SI-10 are calculated for examining the effect of the electrostatic interactions on binding sites of CAs/2 C9 complexes. Figure 10 depicts electrostatic potentials for the residues around the binding sites for A0/CYP2C9 and B0/CYP2C9, respectively. As shown in Fig. 10a, one electronegative phenolic hydroxyl group of A0 lies in an electropositive pocket made of K48, R307, H396, and R357, while the other electronegative phenolic hydroxyl group lies in the electropositive pocket formed by R97 and R94. For B0 of B0/2 C9, there also exist similar electrostatic pockets as shown in Fig. 10b. This leads to the conclusion that the electrostatic interactions may be favorable to the stability of the binding sites of A0-, B0-CYP2C9 complexes.

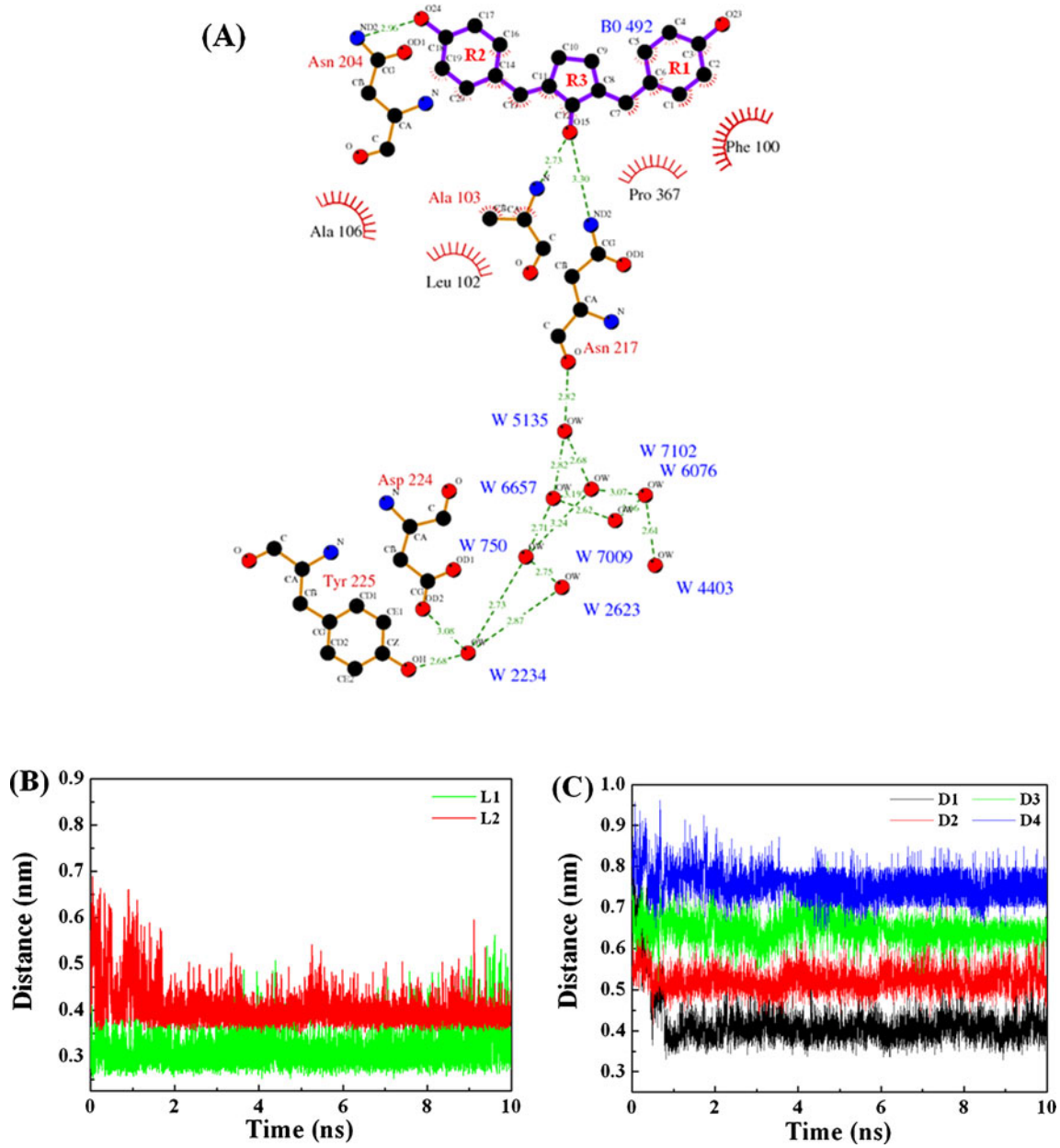

Fig. 7 (**a**) Two-dimensional schematic representation of hydrogen bond and hydrophobic interactions for the binding site of CYP2C9/B0. Red balls represent the oxygen atoms of residues or waters. Black balls and blue balls represent the carbon atoms and nitrogen atoms of residues, respectively. Dashed lines represent hydrogen bonds and spiked residues form hydrophobic interactions. (**b**) Interatomic distances associated with hydrogen bond interaction of B0 in the binding site of CYP2C9 with time evolution. L1 and L2 represent the distances between ketone-oxygen (O15) of B0 and nitrogens of Ala103 and Asn217, respectively. The curve of L2 is shifted upward with 0.1 nm. (**c**) Mass-center distances associated with hydrophobic interactions of B0 in the binding site of CYP2C9 with time evolution. D1 represents the distance between R1 ring of B0 and phenyl ring of Phe100. D3 and D4 display the distances between the R2 ring of B0 and the main chains of Leu102 and Ala106, respectively. D2 represents the distance between R3 rings of B0 and the main chains of Leu102. The curve of D2 is shifted downward by 0.05 nm. The curves of D3 and D4 are shifted upward by 0.05 and 0.2 nm, respectively

Inhibitory effect of CAs on 2C9

According to the results of Vermeulen's group [55], A0 and C0 exhibit strong inhibitory activities with IC_{50} of 1.0 and 1.8 μM, which are comparable with the IC_{50} value 4.3 μM of curcumin. B0 is a moderately strong inhibitor with IC_{50} value of 9.9 μM. However, B12 and C2 are the weak inhibitors to 2 C9 with IC_{50} values of 37.7 and 67.3 μM, respectively. As mentioned above, in the binding sites of A0/2 C9, B0/2 C9, and C0/2 C9, there are stable hydrogen-

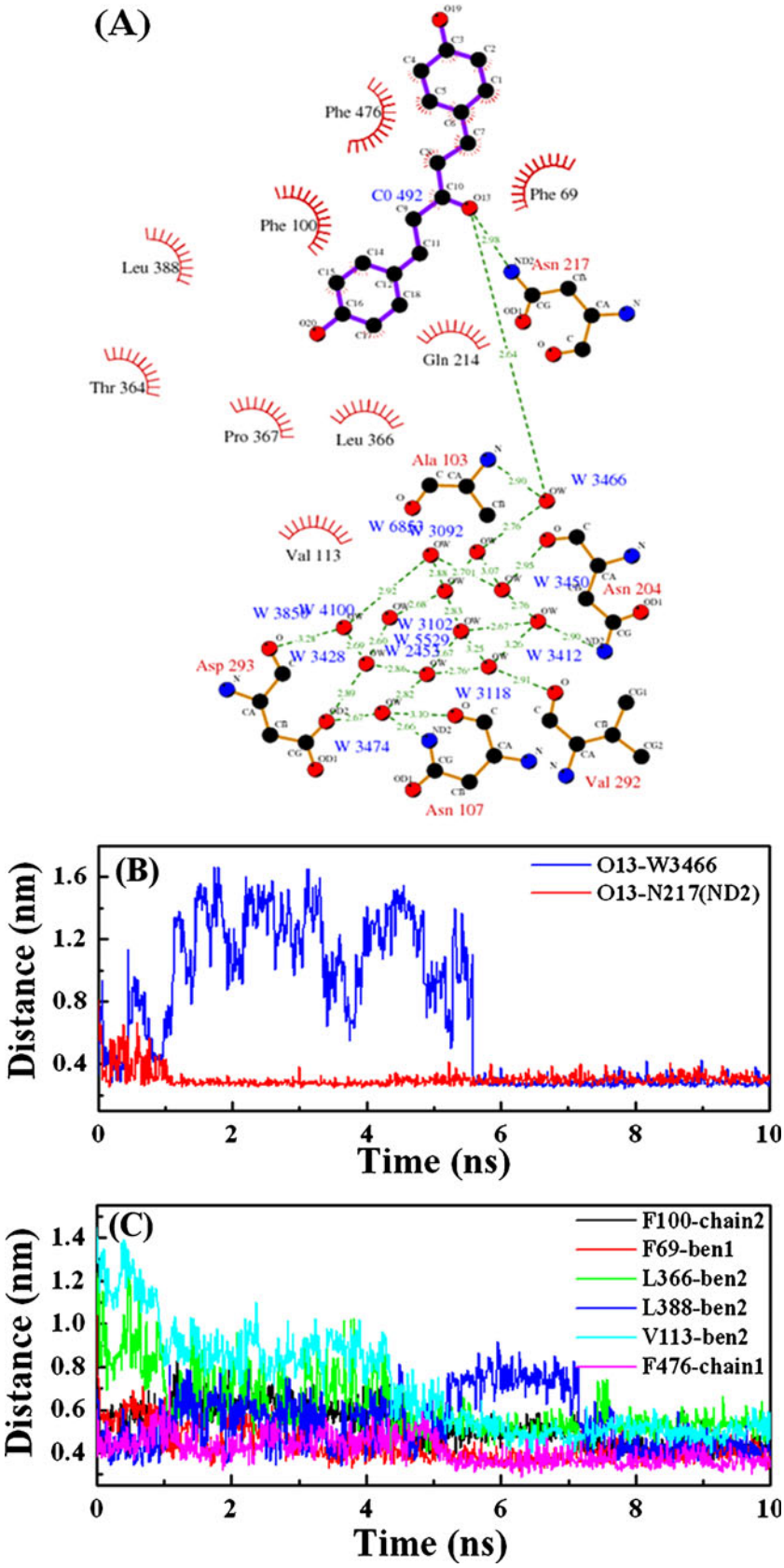

Fig. 8 (**a**) Two-dimensional schematic representation of hydrogen bond and hydrophobic interactions for the binding site of 2 C9/C0. Red balls represent the oxygen atoms of residues or waters. Black balls and blue balls account for the carbon atoms and nitrogen atoms of residues, respectively. Dashed lines represent hydrogen bonds and spiked residues form hydrophobic interactions. (**b**) The H-bond distances between O13 of C0 and a water (W3466) and one nitrogen (ND2) of N217 with time evolution. (**c**) The mass-center distances of hydrophobic residues (F100, F476, F69, L366, L388, V113) with carbon chains (chain1 and chain2) at two sides of the ketone group, two terminal benzene rings (ben1 and ben2) of C0 with time evolution

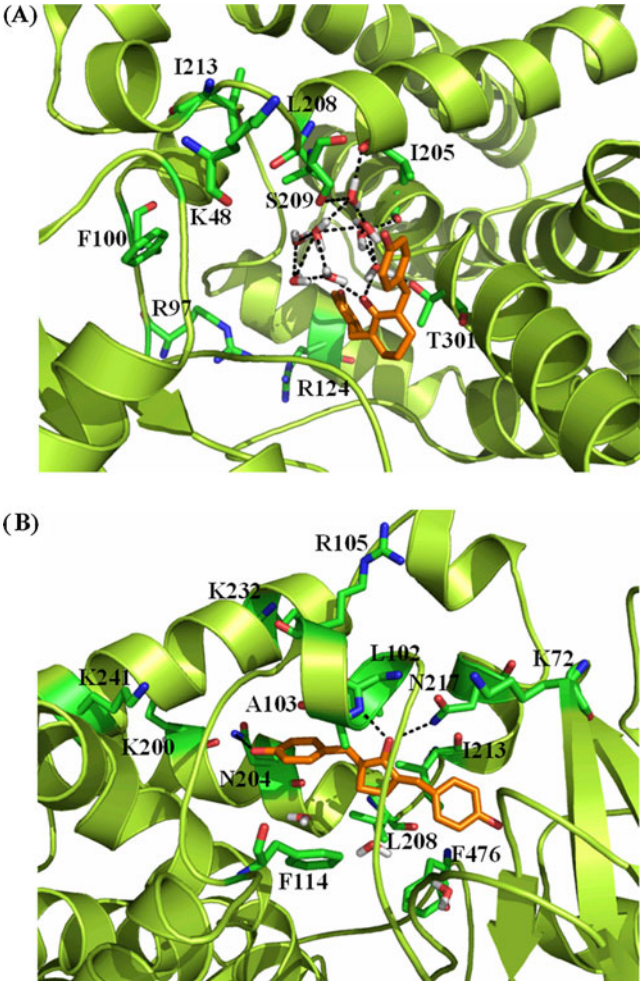

Fig. 9 Final conformations of the binding sites for CYP2C9/A0 (**a**) and CYP2C9/B0 (**b**). Carbon atoms of 2 C9 and ligands (A0 and B0) are colored in limon and green, respectively. Each dotted line (black) indicates a hydrogen bond. The residues and waters surrounding binding sites are shown in sticks

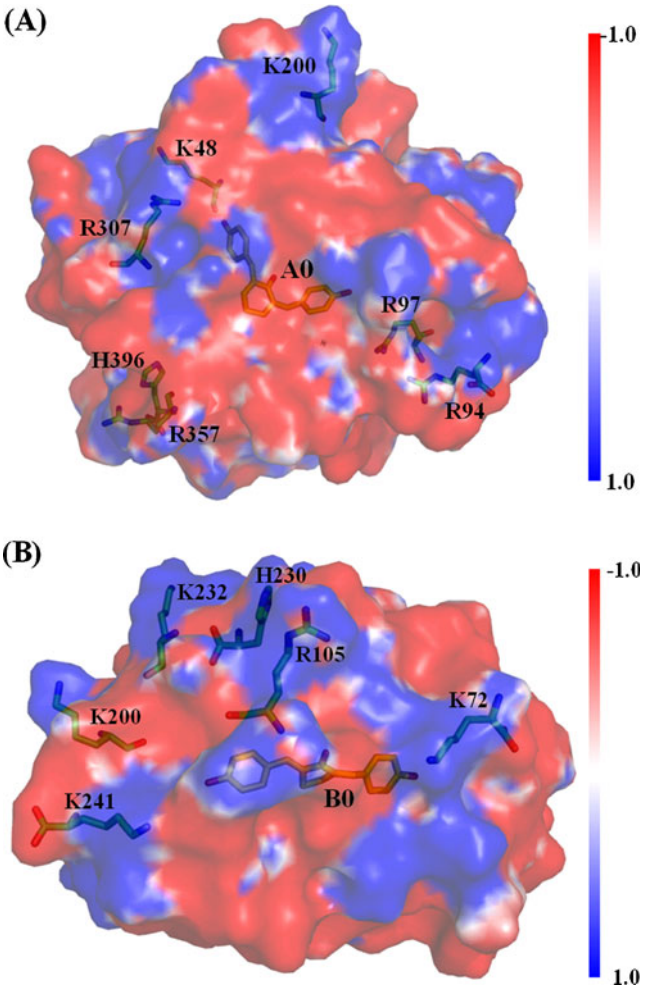

Fig. 10 Electrostatic potentials (−1 to +1 kT/e) for binding sites of CYP2C9/A0 (**a**) and CYP2C9/B0 (**b**). Red, blue, and white represent negative, positive, and neutral regions, respectively

bond and hydrophobic interactions between these CAs and 2 C9. However, it is not the case for B12/2 C9 and C2/2 C9, that is, there are only weak hydrogen-bond and hydrophobic interactions between B12(or C2) and 2 C9. In other words, the interactions in the binding sites of 2 C9-A0,2 C9-B0 and 2 C9-C0 are stronger than those of 2 C9-B12 and 2 C9-C2. It should be noted that our results are qualitatively consistent with the results obtained by Vermeulen's group [55].

Conclusions

In summary, the binding of curcumin analogues with human P450 2 C9 is investigated based on docking and molecular dynamics simulation, which reveals some important features about structures and interactions in binding sites of 2 C9/CAs as follows: (i). the docking results demonstrate that most CAs in current work lie 4~15 Å above the heme of CYP2C9, which is analogous to the results from previous investigations; (ii) the RMSDs, RMSFs,and B-factors reveal that the presence of CAs increases the flexibilities of some residues in bound CYP2C9; (iii) Some CAs undergo conformational changes (from U-bend to extended structures for B0 and C2) in the binding sites of CAs/CYP2C9, which may be caused by the conformational change of binding pocket; (iv) the binding is caused by H-bonds (direct as well as water assisted) and hydrophobic interactions in all the complexes except B12, where only hydrophobic interactions are claimed responsible. On the other hand, there are stable hydrophobic interactions between the phenyl rings of some CAs and some residues of 2 C9. The electrostatic and hydrophobic interactions of A0/2 C9, B0/2 C9, and C0/2 C9 are obviously stronger than those of B12/2 C9 and C2/2 C9,

which is in agreement with the results obtained by Vermeulen's group.

Acknowledgments This work is supported by grants from the National Science Foundation of China (No. 20236010, 20246002, 20376032, 20706029, and 20876073), Jiangsu Science and Technology Department of China (No. BK2008372), and Nanjing University of Technology of China(No. ZK200803). We want to express our thanks for the Reviewers' valuable suggestions for this article.

References

1. Gajendrarao P, Krishnamoorthy N, Sakkiah S, Lazar P, Lee KW (2010) Molecular modeling study on orphan human protein CYP4A22 for identification of potential ligand binding site. J Mol Graphics Model 28:524–532
2. Guengerich FP (2001) Common and uncommon cytochrome P450 reactions related to metabolism and chemical toxicity. Chem Res Toxicol 14:611–650
3. Fishelovitch D, Hazan C, Shaik S, Wolfson HJ, Nussinov R (2007) Structural dynamics of the cooperative binding of organic molecules in the human cytochrome P450 3A4. J Am Chem Soc 129:1603–1611
4. Skopalík J, Anzenbacher P, Otyepka M (2008) Flexibility of human cytochromes P450: Molecular dynamics reveals differences between CYPs 3A4, 2 C9, and 2A6, which correlate with their substrate preferences. J Phys Chem B 112:8165–8173
5. Bathelt CM, Mulholland AJ, Harvey JN (2008) QM/MM modeling of benzene hydroxylation in human cytochrome P450 2 C9. J Phys Chem A 112:13149–13156
6. Ahlström MM, Ridderström M, Zamora I (2007) CYP2C9 structure metabolism relationships: Substrates, inhibitors, and metabolites. J Med Chem 50:5382–5391
7. Eitrich T, Kless A, Druska C, Meyer W, Grotendorst J (2007) Classification of highly unbalanced CYP450 data of drugs using cost sensitive machine learning techniques. J Chem Inf Model 47:92–103
8. Bibi Z (2008) Role of cytochrome P450 in drug interactions. Nutr Metab 5:27–36
9. Afzelius L, Raubacher F, Karlén A, Jørgensen FS, Andersson TB, Masimirembwa CM, Zamora I (2004) Structual analysis of CYP2C9 and CYP2C5 and an evaluation of commonly used molecular modelling techniques. Drug Metab Dispos 32:1218–1229
10. Roberts AG, Cheesman MJ, Primak A, Bowman MK, Atkins WM, Rettie AE (2010) Intramolecular heme ligation of the CYP2C9 R108H mutant demonstrates pronounced conformational flexibility of the B-C loop region: implications for substrate binding. Biochemistry 49:8700–8708
11. Korzekwa KR, Krishnamachary N, Shou M, Ogai A, Parise RA, Rettie AE, Gonzalez FJ, Tracy TS (1998) Evaluation of atypical cytochrome P450 kinetics with two-substrate models: evidence that multiple substrates can simultaneously bind to cytochrome P450 active sites. Biochemistry 37:4137–4147
12. Hutzler JM, Kolwankar D, Hummel MA, Tracy TS (2002) Activation of CYP2C9-mediated metabolism by a series of dapsone analogues: kinetics and structural requirements. Drug Metab Dispos 30:1194–1200
13. Williams PA, Cosme J, Vinkovic DM, Ward A, Angoven HC, Day PJ, Vonrhein C, Tickle IJ, Jhoti H (2004) Crystal structures of human cytochrome P450 3A4 bound to metyrapone and progesterone. Science 305:683–686
14. Yano JK, Wester MR, Schoch GA, Griffin KJ, Stout CD, Johnson EF (2004) The structure of human microsomal cytochrome P450 3A4 determined by X-ray crystallography to 2.05-Å resolution. J Biol Chem 279:38091–38094
15. Williams PA, Cosme J, Ward A, Angove HC, Vinkovic DM, Jhoti H (2003) Crystal structure of human cytochrome P450 2 C9 with bound warfarin. Nature 424:464–468
16. Wester MR, Yano JK, Schoch GA, Yang C, Griffin KJ, Stout CD, Johnson EF (2004) The structure of human cytochrome P450 2 C9 complexed with flurbiprofen at 2.0-Å resolution. J Biol Chem 279:35630–35637
17. Scott EE, He YA, Wester MR, White MA, Chin CC, Halpert JR, Johnson EF, Stout CD (2003) An open conformation of mammalian cytochrome P450 2B4 at 1.6-Å resolution. Proc Natl Acad Sci USA 100:13196–13201
18. Yano JK, Hsu MH, Griffin KJ, Stout CD, Johnson EF (2005) The structure of human microsomal cytochrome P450 2A6 with coumarin and methoxsalen bound. Nat Struct Mol Biol 12:822–823
19. Schoch GA, Yano JK, Wester MR, Griffin KJ, Stout CD, Johnson EF (2004) Structure of human microsomal cytochrome P450 2 C8. J Biol Chem 279:9497–9503
20. Williams PA, Cosme J, Sridhar V, Johnson EF, McRee DE (2000) Mammalian microsomal cytochrome P450 monooxygenase: structural adaptations for membrane binding and functional diversity. Mol Cell 5:121–131
21. Arimoto R (2006) Computational models for predicting interactions with cytochrome P450 enzyme. Curr Top Med Chem 6:1609–1618
22. Kins S, de Groot MJ, Jones JP (2001) Pharmacophore and three dimensional quantitative structure activity relationship methods for modeling cytochrome P450 active sites. Drug Metab Dispos 29:936–944
23. de Graaf C, Vermeulen NP, Feenstra KA (2005) Cytochrome P450 in silico: an integrative modeling approach. J Med Chem 48:2725–2755
24. de Groot MJ, Kirton SB, Sutcliffe MJ (2004) In silico methods for predicting ligand binding determinants of cytochromes P450. Curr Top Med Chem 4:1803–1824
25. Boyer S, Zamora I (2002) New methods in predictive metabolism. J Comput Aided Mol Des 16:403–413
26. de Groot MJ (2006) Designing better drugs: predicting cytochrome P450 metabolism. Drug Discov Today 11:601–606
27. Locuson CW, Rock DA, Jones JP (2004) Quantitative binding models for CYP2C9 based on benzbromarone analogues. Biochemistry 43:6948–6958
28. Yasuo K, Yamaotsu N, Gouda H, Tsujishita H, Hirono S (2009) Structure based CoMFA as a predictive model-CYP2C9 inhibitors as a test case. J Chem Inf Model 49:853–864
29. Yao Y, Han WW, Zhou YH, Li ZS (2007) Molecular docking study of the affinity of CYP2C9 and CYP2D6 for imrecoxib. J Theor Comput Chem 6:541–548
30. Jones DR, Kim SY, Guderyon M, Yun CH, Moran JH, Miller GP (2010) Hydroxywarfarin metabolites potently inhibit CYP2C9 metabolism of S-warfarin. Chem Res Toxicol 23:939–945
31. Aggarwal BB, Kumar A, Bharti AC (2003) Anticancer potential of curcumin: preclinical and clinical studies. Anticancer Res 23:363–398
32. Appiah-Opong R, Commandeur JN, van Vugt-Lussenburg B, Vermeulen NP (2007) Inhibition of human recombinant cytochrome P450s by curcumin and curcumin decomposition products. Toxicology 235:83–91
33. Aggarwal BB, Sundaram C, Malani N, Ichikawa H (2007) Curcumin: the indian solid gold. Adv Exp Med Biol 595:1–75
34. Rao DS, Sekhara NC, Satyanarayana MN, Srinivasan M (1970) Effect of curcumin on serum and liver cholesterol levels in the rat. J Nutr 100:1307–1315
35. Patil TN, Srinivasan M (1971) Hypocholesteremic effect of curcumin in induced hypercholesteremic rats. Indian J Exp Biol 9:167–169

36. Keshavarz K (1976) The influence of turmeric and curcumin on cholesterol concentration of eggs and tissues. Poult Sci 55:1077–1083
37. Soudamini KK, Unnikrishnan MC, Soni KB, Kuttan R (1992) Inhibition of lipid peroxidation and cholesterol levels in mice by curcumin. Indian J Physiol Pharmacol 36:239–243
38. Soni KB, Kuttan R (1992) Effect of oral curcumin administration on serum peroxides and cholesterol levels in human volunteers. Indian J Physiol Pharmacol 36:273–275
39. Hussain MS, Chandrasekhara N (1992) Effect of turmeric on cholesterol gall-stone induction in mice. Indian J Med Res 96:288–291
40. Asai A, Miyazawa T (2001) Dietary curcuminoids prevent high-fat diet-induced lipid accumulation in rat liver and epididymal adipose tissue. J Nutr 131:2932–2935
41. Srivastava R, Puri V, Srimal RC, Dhawan BN (1986) Effect of curcumin on platelet aggregation and vascular prostacyclin synthesis. Arzneimittelforschung 36:715–717
42. Srivastava KC, Bordia A, Verma SK (1995) Curcumin, a major component of food spice turmeric (Curcuma longa) inhibits aggregation and alters eicosanoid metabolism in human blood platelets. Prostag Leukotr Ess 52:223–227
43. Deodhar SD, Sethi R, Srimal RC (1980) Preliminary study on antirheumaticactivity of curcumin. Indian J Med Res 71:632–634
44. Sui Z, Salto R, Li J, Craik C, Ortiz de Montellano PR (1993) Inhibition of the HIV-1 and HIV-2 proteases by curcumin and curcumin boron complexes. Bioorg Med Chem 1:415–422
45. Li CJ, Zhang LJ, Dezube BJ, Crumpacker CS, Pardee AB (1993) Three inhibitors of type 1 human immunodeficiency virus long terminal repeat-directed gene expression and virus replication. Proc Natl Acad Sci USA 90:1839–1842
46. Jordan WC, Drew CR (1996) Curcumin–a natural herb with anti-HIV activity. J Natl Med Assoc 88:333–334
47. Mazumder A, Nearnati N, Sunder S, Schulz J, Pertz H, Eich E, Pommier Y (1997) Curcumin analogs with altered potencies against HIV-1 integrase as probes for biochemical mechanisms of drug action. J Med Chem 40:3057–3063
48. Barthelemy S, Vergnes L, Moynier M, Guyot D, Labidalle S, Bahraoui E (1998) Curcumin and curcumin derivatives inhibit Tat-mediated transactivation of type 1 human immunodeficiency virus long terminal repeat. Res Virol 149:43–52
49. Morikawa T, Matsuda H, Ninomiya K, Yoshikawa M (2002) Medicinal foodstuffs XXIX. Potent protective effects of sesquiterpenes and curcumin from Zedoariae Rhizoma on liver injury induced by D-galactosamine/lipopolysaccharide or tumor necrosis factor-alpha. Biol Pharm Bull 25:627–631
50. Oetari S, Sudibyo M, Commandeur JNM, Samboedi R, Vermeulen NPE (1996) Effects of curcumin on cytochrome P450 and glutathione S-transferase activities in rat liver. Biochem Pharmacol 51:39–45
51. Thapliyal R, Maru GB (2001) Inhibition of cytochrome P450 isozymes by curcumins in vitro and in vivo. Food Chem Toxicol 39:541–547
52. Zhang W, Tan TM, Lim LY (2006) Impact of curcumin induced changes in P-gp and CYP3A4 expression on the pharmacokinetics of peroral celiprolol and midazolam in rats. Drug Metab Dispos 35:110–115
53. Bustanji Y, Taha MO, Almasri IM, Al-Ghussein MAS, Mohammad MK, Alkhatib HS (2009) Inhibition of glycogen synthase kinase by curcumin: investigation by simulated molecular docking and subsequent in vitro/in vivo evaluation. J Enzyme Inhib Med Chem 24:771–778
54. Choi H, Chun YS, Shin YJ, Ye SK, Kim MS, Park JM (2008) Curcumin attenuates cytochrome P450 induction in response to 2,3,7,8-tetrachlorodibenzo-p-dioxin by ROS-dependently degrading AhR and ARNT. Cancer Sci 99:2518–2524
55. Appiah-Opong R, de Esch I, Commandeur JN, Andarini M, Vermeulen NPE (2008) Structure-activity relationships for the inhibition of recombinant human cytochromes P450 by curcumin analogues. Eur J Med Chem 43:1621–1631
56. Firozi PF, Aboobaker VS, Bhattachary RK (1996) Action of curcumin on the cytochrome P450-system catalyzing the activation of aflatoxin B_1. Chem Biol Interact 100:41–51
57. Liu M, Yuan MG, Luo MX, Bu XZ, Luo HB, Hu XP (2010) Binding of curcumin with glyoxalase I: Molecular docking, molecular dynamics simulations, and kinetics analysis. Biophys Chem 147:28–34
58. Sardjiman SS, Reksohadiprodjo MS, Hakim L, van der Goot H, Timmerman H (1997) 1,5-Diphenyl-1,4-pentadiene-3-ones and cyclic analogues as antioxidative agents. Synthesis and structure activity relationship. Eur J Med Chem 32:625–630
59. Frisch MJ, Trucks GW, Schlegel HB, Scuseria GE, Robb MA, Cheeseman JR, Scalmani G, Barone V, Mennucci B, Petersson GA, Nakatsuji H, Caricato M, Li X, Hratchian HP, Izmaylov AF, Bloino J, Zheng G, Sonnenberg JL, Hada M, Ehara M, Toyota K, Fukuda R, Hasegawa J, Ishida M, Nakajima T, Honda Y, Kitao O, Nakai H, Vreven T, Montgomery JA Jr, Peralta JE, Ogliaro F, Bearpark M, Heyd JJ, Brothers E, Kudin KN, Staroverov VN, Kobayashi R, Normand J, Raghavachari K, Rendell A, Burant JC, Iyengar SS, Tomasi J, Cossi M, Rega N, Millam JM, Klene M, Knox JE, Cross JB, Bakken V, Adamo C, Jaramillo J, Gomperts R, Stratmann RE, Yazyev O, Austin AJ, Cammi R, Pomelli C, Ochterski JW, Martin RL, Morokuma K, Zakrzewski VG, Voth GA, Salvador P, Dannenberg JJ, Dapprich S, Daniels AD, Farkas O, Foresman JB Ortiz JV, Cioslowski J, Fox DJ (2009) Gaussian 09 Revision.A.02. Gaussian Inc, Wallingford, CT
60. Morris GM, Goodsell DS, Halliday RS, Huey R, Hart WE, Belew RK, Olson AJ (1998) Automated docking using a Lamarckian genetic algorithnm and an empirical binding free energy function. J Comput Chem 19:1639–1662
61. van der Spoel D, van Buuren AR (1996) Peter Tieleman D, Berendsen HJC (1996) Molecular dynamics simulations of peptides from BPTI: A closer look at amide—aromatic interactions. J Biomol NMR 8:229–238
62. Hermans J, Berendsen HJC, Van Gunsteren WF, Postma JPM (1984) A consistent empirical potential for water-protein interactions. Biopolymers 23:1513–1518
63. Berendsen HJC, van der Spoel D, van Drunen R (1995) GROMACS: a message-passing parallel molecular dynamics implementation. Comput Phys Commun 91:43–56
64. Lindahl E, Hess B, van der Spoel D (2001) GROMACS 3.0: A package for molecular simulation and trajectory analysis. J Mol Mod 7:306–317
65. van Aalten DMF, Bywater R, Findlay JBC, Hendlich M, Hooft RWW, Vriend G (1996) PRODRG, a program for generating molecular topologies and unique molecular descriptors from coordinates of small molecules. J Comput Aided Mol Des 10:255–262
66. Fuhrmans M, Sanders BP, Marrink SJ, de Vries AH (2010) Effects of bundling on the properties of the SPC water mode. Theor Chem Acc 125:335–344
67. Berendsen HJC, Grigera JR, Traatsma TP (1987) The missing term in effective pair potentials. J Phys Chem 91:6269–6271
68. Berendsen HJC, Postma JPM, van Gunsteren WF, DiNola A, Haak JR (1984) Molecular dynamics with coupling to an external bath. J Chem Phys 81:3684–3690
69. Hess B, Bekker H, Berendsen HJC, Fraaije JGEM (1997) LINCS: A linear constraint solver for molecular simulations. J Comput Chem 18:1463–1472

70. Darden T, York D, Pedersen L (1993) Particle mesh Ewald: An N·log(N) method for Ewald sums in large systems. J Chem Phys 98:10089–10092
71. Yao Y, Han WW, Zhou YH, Li ZS, Li Q, Chen XY, Zhong DF (2009) The metabolism of CYP2C9 and CYP2C19 for gliclazide by homology modeling and docking study. Eur J Med Chem 44:854–861
72. Ekroos M, Sjögren T (2006) Structural basis for ligand promiscuity in cytochrome P450 3A4. Proc Natl Acad Sci USA 103:13682–13687
73. Otyepka M, Skopalík J, Anzenbacherová E, Anzenbacher P (2007) What common structural features and variations of mammalian P450s are known to date? Biochim Biophys Acta 1770:376–389
74. Sinha N, Smith-Gill SJ (2002) Electrostatics in protein binding and Function. Curr Protein Pept Sc 3:601–614
75. Weiner PK, Langridge R, Blaney JM, Schaefer R, Kollman PA (1982) Electrostatic potential molecular surfaces. Proc Natl Acad Sci USA 79:3754–3758